J. Math. Computer Sci., 40 (2026), 513–532

Online: ISSN 2008-949X

Journal of Mathematics and Computer Science

Journal Homepage: www.isr-publications.com/jmcs

Feedback-controlled exponential synchronization of a coronary artery chaos system with state and input time-varying delays in complex dynamical networks

Charuwat Chantawat[a], Supreecha Wongaree[b], Naret Ruttanaprommarin[c], Narongsak Yotha[d,*]

[a]*Department of Mathematics and Statistics, Faculty of Science and Technology, Sakon Nakhon Rajabhat University, Sakon Nakhon 47000, Thailand.*

[b]*Institute of General Education, Udon Thani Rajabhat University, Udon Thani 41000, Thailand.*

[c]*Department of Science and Mathematics, Faculty of Industry and Technology, Rajamangala University of Technology Isan, Sakonnakhon Campus, Sakonnakhon 47160, Thailand.*

[d]*Department of Applied Mathematics and Statistics, Faculty of Science and Liberal Arts, Rajamangala University of Technology Isan, Nakhon Ratchasima 30000, Thailand.*

Abstract

The exponential synchronization of the coronary artery chaos system (CACS) in complex dynamical networks (CDNs) with state and input time-varying delays is being studied for the first time. For the CACS in CDNs, feedback control was envisioned. To enable exponential synchronization of the CACS in CDNs with continuous differential time-varying delays, an appropriate Lyapunov-Krasovskii functional (LKF) was constructed. An extended reciprocally convex matrix inequality, Jensen inequality, and Wirtinger-based integral inequality, which further decreases conservativeness, were considered when establishing the synchronization criterion. The new linear matrix inequalities (LMIs) that are required for exponential synchronization have emerged. Numerical checks may be accomplished using MATLAB's LMI toolbox. To demonstrate the efficiency of the recommended strategies, numerical examples were provided.

Keywords: Coronary artery chaos system, complex dynamical networks, exponential synchronization, time-varying delays, feedback control.

2020 MSC: 34C28, 34D06, 34D20.

1. Introduction

Due to the numerous uses of complex dynamical networks (CDNs) in research and engineering, they have received a lot of attention recently, including the study of aviation networks, electricity distribution networks, brain structures, disease transmission networks, the internet, protein interactions, metabolic networks, social interactions, and so on [1, 8, 16, 19, 25, 44]. Typically, CDNs are made up of a large number of nodes, each of which is a group with an associated dynamical system. Depending on the

*Corresponding author

Email addresses: charuwat@snru.ac.th (Charuwat Chantawat), supreechawongaree@udru.ac.th (Supreecha Wongaree), naret.ru@rmuti.ac.th (Naret Ruttanaprommarin), narongsak.yo@rmuti.ac.th (Narongsak Yotha)

doi: 10.22436/jmcs.040.04.05

Received: 2025-05-05 *Revised:* 2025-06-01 *Accepted:* 2025-07-12

network's configuration, some of these nodes are regularly connected. The concept of a graph can be used mathematically to explain these networks. These graphs show the interactions between the vertices and nodes, as edges, each of which is a member of the system.

Many real-world systems, such as those that govern chemical or process operations, electrical engineering systems, transportation systems, the internet, neural networks, etc, frequently experience time delays. This occurs as time delay is a fundamental system characteristic and can lead to instability, oscillations, and deteriorated system performance. As a result, many scholars have become more concerned about the stability of systems that involve time delays during the past twenty years [10, 12, 17, 26, 30]. The delay-independent and delay-dependent criteria can be used to categorize these articles. Delay-independent criteria does not consider the length of the delay, but delay-dependent criteria. When the delay is minor, delay-dependent criteria is generally less antiquated than delay-independent criteria.

The synchronization of chaotic systems also receives a lot of interest in various fields, including biomedicine, electronics, finance, economics, neural networks, and more [20, 37]. Usually, only some nodes for CDNs are constructed simultaneously. It is challenging to identify the condition that may guarantee the synchronization of every node as a consequence. The synchronization control issue is therefore taken into consideration. The several control strategies are suggested in [2–5, 9, 15, 24, 28, 29, 31, 34, 36, 38, 40, 43]. For instance, synchronization performance under quantized sampled-data control for neural networks with random packet dropouts was addressed using enhanced looped functionals in [28]. The authors in [2] investigated mean-square synchronization in neural networks with stochastic sampling and time-varying delays under Markovian jumping parameters. In parallel, the work in [3] tackles secure reachable set synthesis for TS fuzzy semi-Markovian networked systems, offering reliable control mechanisms against cyber-attacks. In [24], the modified function projective synchronization for CDNs with asymmetric coupling and time-varying delays is achieved using the hybrid pinning adaptive control. The synchronized problem of CDNs with hybrid coupling delay is solved in [4] via feedback and intermittent control. Zhao et al. [43] investigated Markovian-directed communication and distributed dynamic event-triggered control for synchronizing Markovian complex networks with input mode delay. In [36], a delayed impulsive control strategy synchronizes complicated networks with unknown constrained time-varying delays. A unique integral inequality-based sampled-data control-based synchronization criteria for CDNs with time-varying coupling delay was studied by Hongsri et al. [15].

Coronary artery chaos system (CACS) synchronization is very significant. CACS is essential to survival because it gives the heart enough oxygen and nutrition throughout the day. As a result, the system's integrity is crucial. Synchronizing the CACS in healthy and diseased individuals is accomplished using several efficient techniques, such as H_∞ control [6, 21–23, 39], mixed passive and H_∞ performance index [13], fuzzy control [32], adaptive control [7, 11, 18, 27], state-feedback control [35], and observer-based control [41]. Especially, Chantawat et al. [6] investigated time-varying input and state delays for finite-time H_∞ synchronization control of CACS. Li et al. [23] used a free-matrix-based integral inequality with time-delay to investigate the H_∞ control for CACS. In [21], the authors looked on synchronizing uncertain CACS with state and time-varying delays under input saturation. Harshavarthini et al. [13] considered the mixed passive and H_∞ performance index finite-time synchronization of the CACS system. Wang et al. [32] researched the state-feedback fuzzy controller for state-time-delayed CACS based on fuzzy models. Li [18] investigated the CACS with an adaptive controller utilizing the backstepping approach to validate the system's local and global bounds. Wu et al. [35] conducted research on the application of CACS for time-varying delay state-feedback synchronization control. In [41], observer-based H_∞ synchronization for a coronary artery time-delay system was investigated under state impedance measurement and external uncertainty. From the above discussions, we can see that the problem of exponential synchronization of the CACS in CDNs with input and state time-varying delays has not been fully investigated yet and remains open. On the other hand, a delay in treatment could have fatal repercussions for a person's life. Additionally, the delay in taking drugs and absorbing their effects impairs system performance and considerably raises the risk to human life. As a result, the treatment's delay is crucial. To ensure that human life is safe, it is essential to forecast and identify a myocardial blockage within a particular amount of

time, particularly in the CACS. Consequently, it is necessary to perceive how the control system operates quickly. Special emergency medications should be taken at a specified moment to prevent the oxygen from the blood from decomposing in the myocardial.

As already mentioned, one of the crucial subjects that needed more research was the synchronization of the CACS in CDNs. Therefore, in this paper, we study the exponential synchronization of CACS in CDNs with time-varying delays. In addition, the article's main contribution may be divided into the following categories.

- For the first time, the issue of exponential synchronization of the CACS in CDNs with state and input time-varying delays is being studied.
- From a theoretical perspective, we mostly employ novel, effective methodologies. For exponential synchronization of CACS in CDNs with input and state time-varying delays, a unique Lyapunov-Krasovskii functional (LKF) is first developed. The value estimation gap is further addressed by proposing an extended reciprocally convex matrix inequality.
- The LKFs constructed in this study consist of single, double, and triple integral terms that utilize more detailed information on delays τ and ρ. These functionals are improved compared to those in recent literature [13, 21, 32, 39, 41], particularly by including triple integral terms, which were not considered in previous works.
- Enhance the standards for CACS synchronization in CDNs with input and state time-varying delays.
- Numerical examples are shown to demonstrate the efficacy of the suggested methodology, which results in less conservatism than the references in [13, 18, 22, 35, 41].

The remainder is divided into four sections in this article. In Section 2, we cover key definitions and lemmas and introduce the CDNs and CACS. For exponential synchronization of the CACS in CDNs with input and state time-varying delays, a novel synchronization criterion is presented in Section 3. Numerical simulations are presented in Section 4 to show the outcomes of the healthy and diseased CACS trajectories. In Section 5, the conclusion is displayed.

2. Problem statement and preliminaries

The following notations are used in this paper. The p-dimensional space is denoted by $\mathbb{R}^p$. Real value matrix of dimension $p \times q$ is represented by $\mathbb{R}^{p\times q}$. The identity matrix is represented by I in the proper dimensions. The transpose of matrix U is referred to as U^T. U is symmetric if $U = U^T$. All of U's eigenvalues are represented by $\lambda(U)$, $\lambda_{max}(U) = \max\{Re\,\lambda : \lambda \in \lambda(U)\}$, and $\lambda_{min}(U) = \min\{Re\,\lambda : \lambda \in \lambda(U)\}$. $U > 0$ or $U < 0$ signifies that the matrix U is symmetric and either a positive or a negative definite matrix. The interpretation of $U > V$ is that $U - V$ is the positive definite matrix if U and V are symmetric. The Euclidean vector norm is superseded by $\|\cdot\|$. $Q = diag\{Q_1, Q_2, \ldots, Q_n\}$ denotes a block diagonal element of matrix Q. $col\{\ldots\}$ denotes a column vector. $*$ stands for the symmetric terms in the matrix. The symbol $\otimes$ represents the Kronecker product.

The following is a description of the CACS mathematical model:

$$\dot{r_1} = -\beta r_1 - d r_2, \quad \dot{r_2} = -(\sigma + \beta\sigma) r_1 - (\sigma + d\sigma) r_2 + \sigma r_1^3 + H\cos\theta t, \tag{2.1}$$

where r_1 represents the variation in the blood vessel's radius, r_2 represents the blood vessel's changing pressure, the periodic stimulating disturbance term is represented by $H\cos\theta t$, and β, d and σ are system parameters. Figure 1 illustrates a control-based synchronization scheme between healthy CACS and diseased CACS.

Based on (2.1), the following describes the diseased CACS in CDNs with coupling for N nodes, each of which is a system of n equations with input time-varying delays:

$$\dot{\eta}_i(t) = A_1\eta_i(t) + A_2\eta_i(t-\tau(t)) + B\mathcal{F}(\eta_i(t)) + G(t) + c\sum_{j=1}^{N} a_{ij}D\eta_i(t) + E\omega_2(t) + u_i(t-\rho(t)). \tag{2.2}$$

The healthy CACS (isolated node) is presented as follows:

$$\dot{s}(t) = A_1 s(t) + A_2 s(t-\tau(t)) + B\mathcal{F}(s(t)) + G(t) + E\omega_1(t), \tag{2.3}$$

where the real constant matrices A_1, A_2, B, and E are given by the values of β, d, σ, and H, $G(t) = [0, 0.3\cos\theta t]$. $\mathcal{F}(s(t)) = [0, s_1^3(t)]$, $\mathcal{F}(\eta_i(t)) = [0, \eta_{i1}^3(t)]$ denotes the nonlinear functions of CACS. $\omega_1(t)$ and $\omega_2(t)$ are the disturbance vectors. $s(t) \in \mathbb{R}^n$ is the state vectors of the healthy CACS. $\eta_i(t) \in \mathbb{R}^n$ is the diseased CACS of the node i. $u_i(t-\rho(t)) \in \mathbb{R}^n$ is input control vector of the node i. The time-varying delay functions in continuous input and state are satisfied:

$$0 \leqslant \tau(t) \leqslant \tau, \qquad \dot{\tau}(t) \leqslant \mu_1, \qquad 0 \leqslant \rho(t) \leqslant \rho, \qquad \dot{\rho}(t) \leqslant \mu_2, \tag{2.4}$$

where τ, ρ, μ_1, and μ_2 are known real constant scalars. The inner-coupling matrix is represented by D, and c specifies a positive constant of coupling strength. The network's outer-coupling matrix, denoted by $A = (a_{ij})_{N\times N} \in \mathbb{R}^{N\times N}$, has the following definition for a_{ij}: if there is an edge between node i and node j $(i \neq j)$; then $a_{ij} = 1$ otherwise, $a_{ij} = 0$ and the diagonal elements of A are specified by

$$a_{ii} = -\sum_{j=1, i\neq j}^{N} a_{ij}, \quad i = 1, 2, \ldots, N.$$

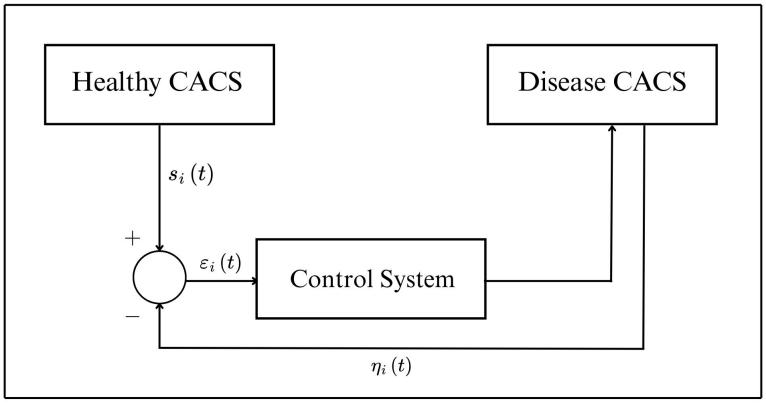

Figure 1: Synchronization diagram of healthy and diseased CACS.

Remark 2.1. The movement of blood and several biochemical processes cause the coronary artery system's delay, which is known as the state time delay. This process is complex. For the sake of investigation, no conditions will modify the state delay, such as drug absorption or other factors during therapy, which is known as the input time delay. In actuality, the amount of medicine absorbed depends on the patient's age, gender, and physical condition. Hence, it is essential to guarantee that the treatment is effective throughout various input time delays. The following study does not assume that the state time delay and the input time delay are related.

The definition of the synchronization error is $\epsilon_i(t) = \eta_i(t) - s(t)$. Using (2.2) and (2.3), we can obtain the error system:

$$\dot{\epsilon}_i(t) = A_1\epsilon_i(t) + A_2\epsilon_i(t-\tau(t)) + Bg(\epsilon_i(t)) + c\sum_{j=1}^{N} a_{ij}D\epsilon_i(t) + E\omega(t) + u_i(t-\rho(t)), \tag{2.5}$$

where $g(\epsilon_i(t)) = \mathcal{F}(\eta_i(t)) - \mathcal{F}(s(t))$, $\omega(t) = \omega_2(t) - \omega_1(t)$.

Assumption 1 ([14]). According to this condition, the continuous function $\mathcal{F} : \mathbb{R}^n \to \mathbb{R}^n$ is satisfied:

$$[\mathcal{F}(x) - \mathcal{F}(y) - G_1(x-y)]^T[\mathcal{F}(x) - \mathcal{F}(y) - G_2(x-y)] \leqslant 0, \ \forall x, y \in \mathbb{R}^n, \tag{2.6}$$

where G_1 and G_2 are compatible-dimension known constant matrices.

By using an appropriate $u_i(t-\rho(t))$ and accounting for the delay in medication administration and absorption, our goal is to synchronize diseased CACS (2.2) and healthy CACS (2.3). The following may be used to design input time-varying delay feedback controllers:

$$u_i(t-\rho(t)) = \bar{K}\epsilon_i(t-\rho(t)), \tag{2.7}$$

where the gain matrix of the control input is $\bar{K}$. The error system is made by combining (2.5) and (2.7),

$$\dot{\epsilon}_i(t) = A_1\epsilon_i(t) + A_2\epsilon_i(t-\tau(t)) + Bg(\epsilon_i(t)) + c\sum_{j=1}^{N} a_{ij}D\epsilon_i(t) + E\omega(t) + \bar{K}\epsilon_i(t-\rho(t)). \tag{2.8}$$

The equation (2.8) can be simplified as the form:

$$\dot{\epsilon}(t) = A_1\epsilon_i(t) + A_2\epsilon_i(t-\tau(t)) + Bg(\epsilon_i(t)) + c(A \otimes D)\epsilon(t) + E\omega(t) + \bar{K}\epsilon_i(t-\rho(t)). \tag{2.9}$$

Remark 2.2. The issue of exponential synchronization of the CACS in CDNs with input and state time-varying delays is being researched for the first time. If $A_2 = 0$ and $c = 0$, the error system (2.5) turns into the error system studied by [13, 18, 22, 35, 41]. We can see that our task already includes the CACS synchronization of the earlier works. This can be seen as an exceptional case of CACS synchronization.

Definition 2.3 ([15]). The closed-loop error system (2.9) is exponentially stable, if there exist two scalars $\nu > 0$ and $\varpi > 0$, such that

$$\|\epsilon(t)\|^2 \leqslant \nu e^{-\varpi t} \sup_{-\max\{\tau,\rho\} \leqslant \theta \leqslant 0} \{\|\epsilon(\theta)\|^2, \|\dot{\epsilon}(\theta)\|^2\}.$$

Definition 2.4 ([6]). Given $\phi > 0$, the error system (2.9) is said to be the H_∞ performance ϕ, if the system is exponentially stable and under zero initial conditions, satisfying

$$\int_0^\infty \epsilon(u)^T\epsilon(u)du \leqslant \phi^2 \int_0^\infty \omega(u)^T\omega(u)du.$$

Lemma 2.5 ([15]). *For any matrix $R > 0$, for derivative functions $\omega \in [\tau_1, \tau_2] \to \mathbb{R}^n$, we obtain*

$$\int_{\tau_1}^{\tau_2} \dot{\omega}^T(s)R\dot{\omega}(s)ds \geqslant \frac{1}{60(\tau_2-\tau_1)}\Sigma^T \begin{bmatrix} 112R & 42R & 72R & -904R \\ * & 158R & -412R & 424R \\ * & * & 1828R & 2976R \\ * & * & * & 6912R \end{bmatrix} \Sigma,$$

where

$$\Sigma = \left[\omega(\tau_2) \ \ \omega(\tau_1) \ \ \frac{1}{\tau_2-\tau_1}\int_{\tau_1}^{\tau_2}\omega(s)ds \ \ \frac{1}{(\tau_2-\tau_1)^2}\int_{\tau_1}^{\tau_2}\int_u^{\tau_2}\omega(s)dsdu\right].$$

Lemma 2.6 ([34]). *Given a matrix $W > 0$, two scalars $0 \leqslant \alpha_1 < \alpha_2$ and vector function $x : [\alpha_1, \alpha_2] \to \mathbb{R}^n$ such that the concerned integrations listed below are well-specified:*

$$\left(\int_{\alpha_1}^{\alpha_2} x(u)du\right)^T W \left(\int_{\alpha_1}^{\alpha_2} x(u)du\right) \leqslant (\alpha_2-\alpha_1)\int_{\alpha_1}^{\alpha_2} x^T(u)Wx(u)du.$$

Lemma 2.7 ([42]). *Given a matrix* $Q > 0$, *scalars* β_1, β_2 *with* $\beta_1 < \beta_2$ *and a continuous differential function* $\phi : [\beta_1, \beta_2] \to \mathbb{R}^n$, *the following integral inequality considerations are made:*

$$\int_{\beta_1}^{\beta_2}\int_{u}^{\beta_2} \dot{\phi}^T(s)Z\dot{\phi}(s)dsdu \geqslant 2\Pi_1^T Q\Pi_1 + 4\Pi_2^T Q\Pi_2 + 6\Pi_3^T Q\Pi_3,$$

where $\kappa = \beta_2 - \beta_1$,

$$\Pi_1 = \phi(\beta_2) - \frac{1}{\kappa}\int_{\beta_1}^{\beta_2}\phi(s)ds,$$
$$\Pi_2 = \phi(\beta_2) + \frac{2}{\kappa}\int_{\beta_1}^{\beta_2}\phi(s)ds - \frac{6}{\kappa^2}\int_{\beta_1}^{\beta_2}\int_{u}^{\beta_2}\phi(s)dsdu,$$
$$\Pi_3 = \phi(\beta_2) - \frac{3}{\kappa}\int_{\beta_1}^{\beta_2}\phi(s)ds + \frac{24}{\kappa^2}\int_{\beta_1}^{\beta_2}\int_{u}^{\beta_2}\phi(s)dsdu - \frac{60}{\kappa^3}\int_{\beta_1}^{\beta_2}\int_{u}^{\beta_2}\int_{r}^{\beta_2}\phi(s)dsdrdu.$$

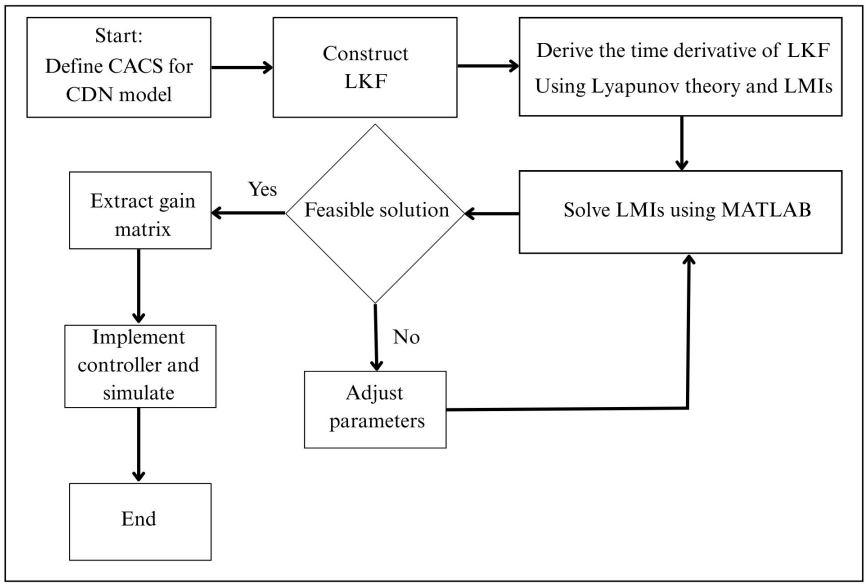

Figure 2: Flowchart of the control design process for CDN based on CACS.

Remark 2.8. Figure 2 presents the flowchart of the control design process for CDN based on CACS. Its illustrates each major step of the method, beginning with system modeling, followed by the construction of LKF, the time derivative of LKF, formulation of LMIs conditions, and verification of the feasibility of these conditions. In situations where a solution cannot be found, the procedure includes adjustment of design parameters such as matrix weights or delay bounds before solving the conditions again. Once feasible gains are obtained, the controller is implemented and the performance of the system is evaluated. This structured process improves readability and makes the design approach more practical for application to complex systems.

3. Main results

Before presenting the main result, the following notations are established for clarity.

$$e_i = [0_{2\times(i-1)2} \;\; I \;\; 0_{2\times(13-i)2}],\; i = 1, 2, \ldots, 13,$$

$$\xi(t) = \mathrm{col}\Big\{ \epsilon(t), \epsilon(t-\tau(t)), \epsilon(t-\tau), \epsilon(t-\rho(t)), \epsilon(t-\rho), \frac{1}{\tau}\int_{t-\tau}^{t} \epsilon(s)ds,$$
$$\frac{1}{\tau^2}\int_{t-\tau}^{t}\int_{s}^{t} \epsilon(u)duds, \frac{1}{\tau^3}\int_{t-\tau}^{t}\int_{u}^{t}\int_{r}^{t} \epsilon(s)dsdrdu, \frac{1}{\rho}\int_{t-\rho}^{t} \epsilon(s)ds,$$
$$\frac{1}{\rho^2}\int_{t-\rho}^{t}\int_{s}^{t} \epsilon(u)duds, \frac{1}{\rho^3}\int_{t-\rho}^{t}\int_{u}^{t}\int_{r}^{t} \epsilon(s)dsdrdu, g(\epsilon(t)), \omega(t)\Big\},$$
$$\zeta_1(t) = -\tau\int_{t-\tau}^{t} \dot\epsilon^T(s)Q_1\dot\epsilon(s)ds - \rho\int_{t-\rho}^{t} \dot\epsilon^T(s)Q_2\dot\epsilon(s)ds, \quad \zeta_2(t) = -\rho\int_{t-\rho}^{t} \dot\epsilon^T(s)Q_3\dot\epsilon(s)ds,$$
$$\zeta_3(t) = \int_{t-\rho}^{t-\rho(t)} \dot\epsilon(s)ds, \qquad \zeta_4(t) = \int_{t-\rho(t)}^{t} \dot\epsilon(s)ds,$$
$$\Gamma_1 = [e_1^T, e_3^T, e_6^T, e_7^T]^T, \quad \Gamma_2 = [e_1^T, e_5^T, e_9^T, e_{10}^T]^T, \quad \Gamma_3 = e_4 - e_5,$$
$$\Gamma_4 = e_1 - e_4, \quad \Gamma_5 = e_1 - e_6, \quad \Gamma_6 = e_1 + 2e_6 - 6e_7,$$
$$\Gamma_7 = e_1 - 3e_6 + 24e_7 - 60e_8, \quad \Gamma_8 = e_1 - e_9, \quad \Gamma_9 = e_1 + 2e_9 - 6e_{10},$$
$$\Gamma_{10} = e_1 - 3e_9 + 24e_{10} - 60e_{11}, \quad \Gamma_{11} = [e_1^T, e_{12}^T]^T,$$
$$\bar G_1 = \frac{(I_N \otimes G_1)^T(I_N \otimes G_2)}{2} + \frac{(I_N \otimes G_2)^T(I_N \otimes G_1)}{2}, \qquad \bar G_2 = -\frac{(I_N \otimes G_1)^T(I_N \otimes G_2)}{2}.$$

The stability criteria for the error system (2.9) with time-varying delays $\tau(t)$ and $\rho(t)$ satisfying (2.4) are now presented.

Theorem 3.1. *Given positive scalars τ, ρ, μ_1, μ_2, υ, any matrix G_1, G_2, the error system (2.9) is exponentially stable, if there exists matrices $P > 0$, $R_1 > 0$,$R_2 > 0$, $R_3 > 0$, $R_4 > 0$, $Q_1 > 0$, $Q_2 > 0$, $Q_3 > 0$, $T_1 > 0$, $T_2 > 0$, for any matrix Q with appropriate dimension such that the following conditions hold:*

$$\begin{bmatrix} Q_3 & Q \\ * & Q_3 \end{bmatrix} \geqslant 0, \quad \Pi = \begin{bmatrix} \Pi_{11} & \Pi_{12} \\ * & \Pi_{22} \end{bmatrix} < 0, \tag{3.1}$$

where

$$\Pi_{11} = \vartheta_1 + \vartheta_2 + \vartheta_3 + \vartheta_4 + \vartheta_5 - \upsilon\Gamma_{11}^T \begin{bmatrix} \bar G_1 & \bar G_2 \\ * & I \end{bmatrix} \Gamma_{11},$$
$$\Pi_{12} = [\tau\Upsilon^T Q_1, \rho\Upsilon^T Q_2, \rho\Upsilon^T Q_3, \frac{\tau}{\sqrt{2}}\Upsilon^T T_1, \frac{\rho}{\sqrt{2}}\Upsilon^T T_2],$$
$$\Pi_{22} = \mathrm{diag}\{-Q_1, -Q_2, -Q_3, -T_1, -T_2\},$$
$$\Upsilon = A_1e_1 + A_2e_2 + Be_{12} + c(A \otimes D)e_1 + \bar K e_4 + Ee_{13},$$
$$\vartheta_1 = e_1^T[P + P^T]\Upsilon,$$
$$\vartheta_2 = e_1^T(R_1 + R_2 + R_3 + R_4)e_1 - (1-\mu_1)e_2^T R_1 e_2 - (1-\mu_2)e_4^T R_3 e_4 - e_3^T R_2 e_3 - e_5^T R_4 e_5,$$
$$\vartheta_3 = -\Gamma_1^T M_1 \Gamma_1 - \Gamma_2^T M_2 \Gamma_2,$$
$$\vartheta_4 = -\Gamma_3^T Q_3\Gamma_3 - \Gamma_4^T Q_3\Gamma_4 - \Gamma_3^T Q\Gamma_4 - \Gamma_4^T Q^T\Gamma_3,$$
$$\vartheta_5 = -2\Gamma_5^T T_1\Gamma_5 - 4\Gamma_6^T T_1\Gamma_6 - 6\Gamma_7^T T_1\Gamma_7 - 2\Gamma_8^T T_2\Gamma_8 - 4\Gamma_9^T T_2\Gamma_9 - 6\Gamma_{10}^T T_2\Gamma_{10},$$
$$M_1 = \frac{1}{60}\begin{bmatrix} 112Q_1 & 42Q_1 & 72Q_1 & -904Q_1 \\ * & 158Q_1 & -412Q_1 & 424Q_1 \\ * & * & 1828Q_1 & 2976Q_1 \\ * & * & * & 6912Q_1 \end{bmatrix},$$

$$M_2 = \frac{1}{60}\begin{bmatrix} 112Q_2 & 42Q_2 & 72Q_2 & -904Q_2 \\ * & 158Q_2 & -412Q_2 & 424Q_2 \\ * & * & 1828Q_2 & 2976Q_2 \\ * & * & * & 6912Q_2 \end{bmatrix}.$$

Proof. The error system (2.9) takes into account the following LKF:

$$V(\epsilon(t)) = \sum_{i=1}^{4} V_i(\epsilon(t)), \tag{3.2}$$

where

$$\begin{aligned}
V_1(\epsilon(t)) &= \epsilon^T(t)P\epsilon(t),\\
V_2(\epsilon(t)) &= \int_{t-\tau(t)}^{t} \epsilon^T(s)R_1\epsilon(s)ds + \int_{t-\tau}^{t} \epsilon^T(s)R_2\epsilon(s)ds + \int_{t-\rho(t)}^{t} \epsilon^T(s)R_3\epsilon(s)ds + \int_{t-\rho}^{t} \epsilon^T(s)R_4\epsilon(s)ds,\\
V_3(\epsilon(t)) &= \tau\int_{-\tau}^{0}\int_{t+\theta}^{t} \dot\epsilon^T(s)Q_1\dot\epsilon(s)ds d\theta + \rho\int_{-\rho}^{0}\int_{t+\theta}^{t} \dot\epsilon^T(s)Q_2\dot\epsilon(s)ds d\theta + \rho\int_{-\rho}^{0}\int_{t+\theta}^{t} \dot\epsilon^T(s)Q_3\dot\epsilon(s)ds d\theta,\\
V_4(\epsilon(t)) &= \int_{t-\tau}^{t}\int_{\theta}^{t}\int_{r}^{t} \dot\epsilon^T(s)T_1\dot\epsilon(s)ds dr d\theta + \int_{t-\rho}^{t}\int_{\theta}^{t}\int_{r}^{t} \dot\epsilon^T(s)T_2\dot\epsilon(s)ds dr d\theta.
\end{aligned}$$

It is possible to derive the time derivative of $V(\epsilon(t))$ in (3.2):

$$\begin{aligned}
\dot V_1(\epsilon(t)) &= 2\epsilon^T(t)P\dot\epsilon(t) = \xi^T(t)\vartheta_1\xi(t),\\
\dot V_2(\epsilon(t)) &\leqslant \epsilon^T(t)[R_1+R_2+R_3+R_4]\epsilon(t) - (1-\mu_1)\epsilon^T(t-\tau(t))R_1\epsilon(t-\tau(t))\\
&\quad - \epsilon^T(t-\tau)R_2\epsilon(t-\tau) - (1-\mu_2)\epsilon^T(t-\rho(t))R_3\epsilon(t-\rho(t)) - \epsilon^T(t-\rho)R_4\epsilon(t-\rho)\\
&= \xi^T(t)\vartheta_2\xi(t),\\
\dot V_3(\epsilon(t)) &= \dot\epsilon^T(t)[\tau^2Q_1+\rho^2Q_2+\rho^2Q_3]\dot\epsilon(t) - \tau\int_{t-\tau}^{t} \dot\epsilon^T(s)Q_1\dot\epsilon(s)ds\\
&\quad - \rho\int_{t-\rho}^{t} \dot\epsilon^T(s)Q_2\dot\epsilon(s)ds - \rho\int_{t-\rho}^{t} \dot\epsilon^T(s)Q_3\dot\epsilon(s)ds,\\
\dot V_4(\epsilon(t)) &= \dot\epsilon^T(t)\left[\frac{\tau^2}{2}T_1 + \frac{\rho^2}{2}T_2\right]\dot\epsilon(t) - \int_{t-\tau}^{t}\int_{r}^{t} \dot\epsilon^T(s)T_1\dot\epsilon(s)ds dr - \int_{t-\rho}^{t}\int_{r}^{t} \dot\epsilon^T(s)T_2\dot\epsilon(s)ds dr.
\end{aligned} \tag{3.3}$$

Using Lemma 2.5, we get

$$\begin{aligned}
\zeta_1(t) &\leqslant -\frac{1}{60}\left[\epsilon^T(t), \epsilon^T(t-\tau), \frac{1}{\tau}\int_{t-\tau}^{t}\epsilon^T(s)ds, \frac{1}{\tau^2}\int_{t-\tau}^{t}\int_{s}^{t}\epsilon^T(u)du ds\right]M_1\\
&\quad\times\left[\epsilon^T(t), \epsilon^T(t-\tau), \frac{1}{\tau}\int_{t-\tau}^{t}\epsilon^T(s)ds, \frac{1}{\tau^2}\int_{t-\tau}^{t}\int_{s}^{t}\epsilon^T(u)du ds\right]^T\\
&\quad-\frac{1}{60}\left[\epsilon^T(t), \epsilon^T(t-\rho), \frac{1}{\rho}\int_{t-\rho}^{t}\epsilon^T(s)ds, \frac{1}{\rho^2}\int_{t-\rho}^{t}\int_{s}^{t}\epsilon^T(u)du ds\right]M_2\\
&\quad\times\left[\epsilon^T(t), \epsilon^T(t-\rho), \frac{1}{\rho}\int_{t-\rho}^{t}\epsilon^T(s)ds, \frac{1}{\rho^2}\int_{t-\rho}^{t}\int_{s}^{t}\epsilon^T(u)du ds\right]^T = \xi^T(t)\vartheta_3\xi(t).
\end{aligned} \tag{3.4}$$

Next, when $0 \leqslant \rho(t) \leqslant \rho$, we have

$$\rho\int_{t-\rho}^{t} \dot\epsilon^T(s)Q_3\dot\epsilon(s)ds = \rho\int_{t-\rho}^{t-\rho(t)} \dot\epsilon^T(s)Q_3\dot\epsilon(s)ds + \rho\int_{t-\rho(t)}^{t} \dot\epsilon^T(s)Q_3\dot\epsilon(s)ds. \tag{3.5}$$

Using Lemma 2.6, we get

$$\rho\int_{t-\rho}^{t-\rho(t)}\dot{e}^T(s)Q_3\dot{e}(s)ds \geqslant \frac{\rho}{\rho-\rho(t)}\zeta_3^T(t)Q_3\zeta_3(t), \quad \rho\int_{t-\rho(t)}^{t}\dot{e}^T(s)Q_3\dot{e}(s)ds \geqslant \frac{\rho}{\rho(t)}\zeta_4^T(t)Q_3\zeta_4(t).$$

Now, we have

$$\begin{aligned}
&\rho\int_{t-\rho}^{t}\dot{e}^T(s)Q_3\dot{e}(s)ds \\
&\geqslant \frac{\rho}{\rho-\rho(t)}\zeta_3^T(t)Q_3\zeta_3(t)+\frac{\rho}{\rho(t)}\zeta_4^T(t)Q_3\zeta_4(t) \\
&= \zeta_3^T(t)Q_3\zeta_3(t)+\frac{\rho(t)}{\rho-\rho(t)}\zeta_3^T(t)Q_3\zeta_3(t)+\zeta_4^T(t)Q_3\zeta_4(t)+\frac{\rho-\rho(t)}{\rho(t)}\zeta_4^T(t)Q_3\zeta_4(t).
\end{aligned} \tag{3.6}$$

By reciprocally convex with $p=\frac{\rho-\rho(t)}{\rho}$, $q=\frac{\rho(t)}{\rho}$, the following inequality holds:

$$\begin{bmatrix} \sqrt{\frac{q}{p}}\zeta_3(t) \\ -\sqrt{\frac{p}{q}}\zeta_4(t) \end{bmatrix}^T \begin{bmatrix} Q_3 & Q \\ Q^T & Q_3 \end{bmatrix} \begin{bmatrix} \sqrt{\frac{q}{p}}\zeta_3(t) \\ -\sqrt{\frac{p}{q}}\zeta_4(t) \end{bmatrix} \geqslant 0, \tag{3.7}$$

which implies

$$\frac{\rho(t)}{\rho-\rho(t)}\zeta_3^T(t)Q_3\zeta_3(t)+\frac{\rho-\rho(t)}{\rho(t)}\zeta_4^T(t)Q_3\zeta_4(t) \geqslant \zeta_3^T(t)Q\zeta_4(t)+\zeta_4^T(t)Q^T\zeta_3(t), \tag{3.8}$$

then, we can get from (3.5)-(3.8) that

$$\zeta_2(t) \leqslant -\zeta_3^T(t)Q_3\zeta_3(t)-\zeta_4^T(t)Q_3\zeta_4(t)-\zeta_3^T(t)Q\zeta_4(t)-\zeta_4^T(t)Q^T\zeta_3(t)=\xi^T(t)\vartheta_4\xi(t).$$

Using Lemma 2.7, we obtain

$$-\int_{t-\tau}^{t}\int_{r}^{t}\dot{e}^T(s)T_1\dot{e}(s)dsdr-\int_{t-\rho}^{t}\int_{r}^{t}\dot{e}^T(s)T_2\dot{e}(s)dsdr \leqslant \xi^T(t)\vartheta_5\xi(t). \tag{3.9}$$

From the relation (2.6), it is obvious that the nonlinear function $g(e(t))$, for any $\upsilon>0$ satisfies

$$-\upsilon\begin{bmatrix} e(t) \\ g(e(t)) \end{bmatrix}^T \begin{bmatrix} \bar{G}_1 & \bar{G}_2 \\ * & I \end{bmatrix} \begin{bmatrix} e(t) \\ g(e(t)) \end{bmatrix} \geqslant 0. \tag{3.10}$$

Combining (3.3)-(3.10), we get

$$\dot{V}(\epsilon(t)) \leqslant \xi^T(t)\Pi\xi(t), \tag{3.11}$$

which suggests that for a small $\gamma>0$ sufficient amount, $\dot{V}(\epsilon(t)) \leqslant -\gamma\|\epsilon(t)\|^2$. Moreover, according to the definitions of $V_i(\epsilon(t))$, the following inequalities are simple to obtain:

$$V_1(\epsilon(t)) \leqslant \lambda_{max}(P)\|\epsilon(t)\|^2, \tag{3.12}$$

$$V_2(\epsilon(t)) \leqslant \int_{t-\tau}^{t}\epsilon^T(s)R_1\epsilon(s)ds+\int_{t-\tau}^{t}\epsilon^T(s)R_2\epsilon(s)ds+\int_{t-\rho}^{t}\epsilon^T(s)R_3\epsilon(s)ds+\int_{t-\rho}^{t}\epsilon^T(s)R_4\epsilon(s)ds, \tag{3.13}$$

$$V_3(\epsilon(t)) \leqslant \tau^2\int_{t-\tau}^{t}\dot{e}^T(s)Q_1\dot{e}(s)ds+\rho^2\int_{t-\rho}^{t}\dot{e}^T(s)Q_2\dot{e}(s)ds+\rho^2\int_{t-\rho}^{t}\dot{e}^T(s)Q_3\dot{e}(s)ds, \tag{3.14}$$

$$V_4(\epsilon(t)) \leqslant \frac{\tau^2}{2}\int_{t-\tau}^{t}\dot{e}^T(s)T_1\dot{e}(s)ds+\frac{\rho^2}{2}\int_{t-\rho}^{t}\dot{e}^T(s)T_2\dot{e}(s)ds. \tag{3.15}$$

The exponential stability of (2.9) is being investigated. We consider the LKF $e^{2\alpha t}V(\epsilon(t))$, where α is a constant to be identified. From (3.11)-(3.15), we have

$$\begin{aligned}\frac{d}{dt}e^{2\alpha t}V(\epsilon(t)) &= e^{2\alpha t}\dot{V}(\epsilon(t)) + 2\alpha e^{2\alpha t}V(\epsilon(t))\\ &\leqslant e^{2\alpha t}\Big[-\gamma + 2\alpha\Big(\lambda_{max}(P) + \tau\lambda_{max}(R_1) + \tau\lambda_{max}(R_2) + \rho\lambda_{max}(R_3)\\ &\quad + \rho\lambda_{max}(R_4) + \tau^3\lambda_{max}(Q_1) + \rho^3\lambda_{max}(Q_2) + \rho^3\lambda_{max}(Q_3) + \frac{\tau^3}{2}\lambda_{max}(T_1)\\ &\quad + \frac{\rho^3}{2}\lambda_{max}(T_2)\Big)\Big] \sup_{-\max\{\tau,\rho\}\leqslant\theta\leqslant 0}\{||\epsilon(t+\theta)||^2, ||\dot{\epsilon}(t+\theta)||^2\}.\end{aligned} \tag{3.16}$$

Let

$$\rho_0 = \rho_1 + \rho_2 + \rho_3 + \rho_4, \quad \rho_1 = \lambda_{max}(P), \quad \rho_2 = \tau\lambda_{max}(R_1) + \tau\lambda_{max}(R_2) + \rho\lambda_{max}(R_3) + \rho\lambda_{max}(R_4),$$
$$\rho_3 = \tau^3\lambda_{max}(Q_1) + \rho^3\lambda_{max}(Q_2) + \rho^3\lambda_{max}(Q_3), \quad \rho_4 = \frac{\tau^3}{2}\lambda_{max}(T_1) + \frac{\rho^3}{2}\lambda_{max}(T_2).$$

Thus, we assume that α is a constant that satisfies the condition $\alpha \leqslant \frac{\gamma}{2\rho_0}$ and we derive from (3.16) that

$$\frac{d}{dt}e^{2\alpha t}V(\epsilon(t)) \leqslant 0,$$

which, together with (3.12)-(3.15), indicates that

$$\begin{aligned}e^{2\alpha t}V(\epsilon(t)) \leqslant V(\epsilon(0)) &= \sum_{i=1}^{4} V_i(\epsilon(0))\\ &\leqslant \lambda_{max}(P)||\epsilon(0)||^2 + \int_{-\tau}^{0}\epsilon^T(s)R_1\epsilon(s)ds + \int_{-\tau}^{0}\epsilon^T(s)R_2\epsilon(s)ds + \int_{-\rho}^{0}\epsilon^T(s)R_3\epsilon(s)ds\\ &\quad + \int_{-\rho}^{0}\epsilon^T(s)R_4\epsilon(s)ds + \tau^2\int_{-\tau}^{0}\dot{\epsilon}^T(s)Q_1\dot{\epsilon}(s)ds + \rho^2\int_{-\rho}^{0}\dot{\epsilon}^T(s)Q_2\dot{\epsilon}(s)ds\\ &\quad + \rho^2\int_{-\rho}^{0}\dot{\epsilon}^T(s)Q_3\dot{\epsilon}(s)ds + \frac{\tau^2}{2}\int_{-\tau}^{0}\dot{\epsilon}^T(s)T_1\dot{\epsilon}(s)ds + \frac{\rho^2}{2}\int_{-\rho}^{0}\dot{\epsilon}^T(s)T_2\dot{\epsilon}(s)ds\\ &\leqslant \rho_0 \sup_{-\max\{\tau,\rho\}\leqslant\theta\leqslant 0}\{||\epsilon(\theta)||^2, ||\dot{\epsilon}(\theta)||^2\},\end{aligned}$$

thus

$$V(\epsilon(t)) \leqslant \rho_0 e^{-2\alpha t} \sup_{-\max\{\tau,\rho\}\leqslant\theta\leqslant 0}\{||\epsilon(\theta)||^2, ||\dot{\epsilon}(\theta)||^2\}.$$

Because $V(\epsilon(t)) \geqslant V_1(\epsilon(t)) \geqslant \lambda_{min}(P)||\epsilon(t)||^2$, we get

$$||\epsilon(t)||^2 \leqslant \frac{\rho_0}{\lambda_{min}(P)}e^{-2\alpha t} \sup_{-\max\{\tau,\rho\}\leqslant\theta\leqslant 0}\{||\epsilon(\theta)||^2, ||\dot{\epsilon}(\theta)||^2\}. \tag{3.17}$$

By letting $\nu = \frac{\rho_0}{\lambda_{min}(P)}$ and $\varpi = 2\alpha$, (3.17) can be changed to

$$||\epsilon(t)||^2 \leqslant \nu e^{-\varpi t} \sup_{-\max\{\tau,\rho\}\leqslant\theta\leqslant 0}\{||\epsilon(\theta)||^2, ||\dot{\epsilon}(\theta)||^2\}.$$

Hence, system (2.9) exhibits exponentially stable. The proof has been completed. □

Remark 3.2. The LKFs in this study are made up of single, double, and triple integral terms that use further information on the delays τ and ρ. We enhanced the LKFs which are different from those that have been published recently [13, 21, 32, 39, 41]. Furthermore, the LKFs with the triple integral term $\int_{t-\tau}^{t}\int_{\theta}^{t}\int_{r}^{t}\dot{e}^{T}(s)T_1\dot{e}(s)dsdrd\theta+\int_{t-\rho}^{t}\int_{\theta}^{t}\int_{r}^{t}\dot{e}^{T}(s)T_2\dot{e}(s)dsdrd\theta$ were not utilized in [13, 21, 32, 39, 41]. Less conservatism is achieved by constructing improved LKFs and using methods for estimating the time derivatives.

Remark 3.3. A standard for assessing the stability of error systems built on an unsolved $\bar{K}$ is provided by Theorem 3.1. The following theorem is suitable conditions that can be given to solve the matrix $\bar{K}$ problem.

Theorem 3.4. *For given positive scalars τ, ρ, μ_1, μ_2, υ, any matrix G_1, G_2, the error system (2.9) is exponentially synchronized by the feedback controller (2.7), if there exists matrices $P=\operatorname{diag}\{P_1,P_2,\ldots,P_N\}>0$, $R_1>0$,$R_2>0$, $R_3>0$, $R_4>0$, $Q_1>0$, $Q_2>0$, $Q_3>0$, $T_1>0$, $T_2>0$, $X=\operatorname{diag}\{X_1,X_2,\ldots,X_N\}$, for any matrix Q with appropriate dimension such that the following conditions hold:*

$$\begin{bmatrix} Q_3 & Q \\ * & Q_3 \end{bmatrix} \geqslant 0, \tag{3.18}$$

$$\bar{\Pi}=\begin{bmatrix} \bar{\Pi}_{11} & \bar{\Pi}_{12} \\ * & \bar{\Pi}_{22} \end{bmatrix} < 0, \tag{3.19}$$

where

$$\begin{aligned}
\bar{\Pi}_{11} &= \vartheta_1+\vartheta_2+\vartheta_3+\vartheta_4+\vartheta_5-\upsilon\Gamma_{11}^{T}\begin{bmatrix} \bar{G}_1 & \bar{G}_2 \\ * & I \end{bmatrix}\Gamma_{11}+e_1^{T}Ie_1-\phi^2e_{13}^{T}Ie_{13},\\
\bar{\Pi}_{12} &= [\tau\bar{\Upsilon}^{T},\rho\bar{\Upsilon}^{T},\rho\bar{\Upsilon}^{T},\frac{\tau}{\sqrt{2}}\bar{\Upsilon}^{T},\frac{\rho}{\sqrt{2}}\bar{\Upsilon}^{T}],\\
\bar{\Pi}_{22} &= \operatorname{diag}\{-2P+Q_1,-2P+Q_2,-2P+Q_3,-2P+T_1,-2P+T_2\},\\
\bar{\Upsilon} &= PA_1e_1+PA_2e_2+PBe_{12}+Pc(A\otimes D)e_1+Xe_4+PEe_{13},
\end{aligned}$$

and the definitions for the additional variables match those in Theorem 3.1. Additionally, the gain matrices of the necessary controllers are provided by $\bar{K}=P^{-1}X$.

Proof. In this theorem, the H_∞ performance will be demonstrated. This theorem's proof follows as a result of Theorem 3.1 throughout the entirety. Now, for any nonzero disturbance $\omega(t)$, it is straightforward to derive by using the same LKF candidate (3.2) in Theorem 3.1,

$$\dot{V}(\epsilon(t))+\epsilon^{T}(t)\epsilon(t)-\phi^2\omega^{T}(t)\omega(t)\leqslant\xi^{T}(t)\bar{\Pi}_{11}\xi(t).$$

By setting $X=P\bar{K}$ and defining

$$\mathcal{T}=\operatorname{diag}\{\overbrace{I,\ldots,I}^{13},PQ_1^{-1},PQ_2^{-1},PQ_3^{-1},PT_1^{-1},PT_2^{-1}\}$$

afterward, by pre- and post-multiplying (3.1) with $\mathcal{T}$ and $\mathcal{T}^{T}$, respectively, we achieve that the inequality (3.1) is equivalent to

$$\begin{bmatrix} \bar{\Pi}_{11} & \bar{\Pi}_{12} \\ * & \hat{\Pi}_{22} \end{bmatrix} < 0, \tag{3.20}$$

where

$$\hat{\Pi}_{22}=\operatorname{diag}\{-PQ_1^{-1}P,-PQ_2^{-1}P,-PQ_3^{-1}P,-PT_1^{-1}P,-PT_2^{-1}P\}.$$

Noting $Q_1>0$, we have $-PQ_1^{-1}P\leqslant-2P+Q_1$, in a similar way, $Q_2>0$, $Q_3>0$, $T_1>0$, and $T_2>0$ and we have $-PQ_2^{-1}P\leqslant-2P+Q_2$, $-PQ_3^{-1}P\leqslant-2P+Q_3$, $-PT_1^{-1}P\leqslant-2P+T_1$ and $-PT_2^{-1}P\leqslant-2P+T_2$, respectively. We obtain (3.19) and the proof is now complete. □

Remark 3.5. In addition to the method shown above, the inequality (3.20) involves nonlinear terms, specifically $\hat{\Pi}_{22} = \text{diag}\{-PQ_1^{-1}P, -PQ_2^{-1}P, -PQ_3^{-1}P, -PT_1^{-1}P, -PT_2^{-1}P\}$. To obtain feasible solutions to this problem, the cone complementary linearisation (CCL) [33] approach can be employed . Hence, the inequality (3.20) can be modified using the iterative algorithm. Firstly, we define new variables $\mathfrak{U}_i (j = 1, 2, 3)$ and $\mathcal{Z}_j (j = 1, 2)$, such that

$$PQ_i^{-1}P \geqslant \mathfrak{U}_i \ (i = 1, 2, 3), \quad PT_j^{-1}P \geqslant \mathcal{Z}_j \ (j = 1, 2),$$

which can be transformed to

$$\begin{bmatrix} -Q_i^{-1} & P^{-1} \\ * & -\mathfrak{U}_i^{-1} \end{bmatrix} \leqslant 0 \ (i = 1, 2, 3), \quad \begin{bmatrix} -T_j^{-1} & P^{-1} \\ * & -\mathcal{Z}_j^{-1} \end{bmatrix} \leqslant 0 \ (j = 1, 2).$$

By introducing variables $P^{-1} = \mathfrak{P}$, $Q_i^{-1} = \mathcal{J}_i$, $\mathfrak{U}_i^{-1} = \mathfrak{H}_i, (i = 1, 2, 3)$, $T_j^{-1} = \mathcal{L}_j$, $\mathcal{Z}_j^{-1} = \mathcal{W}_j, (j = 1, 2)$, which is equivalent to

$$\begin{bmatrix} -\mathcal{J}_i & \mathfrak{P} \\ * & -\mathfrak{H}_i \end{bmatrix} \leqslant 0 \ (i = 1, 2, 3), \quad \begin{bmatrix} -\mathcal{L}_j & \mathfrak{P} \\ * & -\mathcal{W}_j \end{bmatrix} \leqslant 0 \ (j = 1, 2).$$

According to the CCL, the original problem of Theorem 3.4 can be replaced by the following minimization problem. Minimize

$$\text{tr}\left(\mathfrak{P}P + \sum_{i=1}^{3}(\mathcal{J}_i Q_i + \mathfrak{H}_i \mathfrak{U}_i) + \sum_{j=1}^{2}(\mathcal{L}_j T_j + \mathcal{W}_j \mathcal{Z}_j)\right),$$

subject to (3.18), (3.19), and

$$\bar{\Pi} = \begin{bmatrix} \bar{\Pi}_{11} & \bar{\Pi}_{12} \\ * & \mathcal{M}_{22} \end{bmatrix} < 0, \quad \begin{bmatrix} \mathfrak{P} & I \\ * & P \end{bmatrix} \geqslant 0,$$
$$\begin{bmatrix} \mathcal{J}_i & I \\ * & Q_i \end{bmatrix} \geqslant 0, \quad \begin{bmatrix} \mathfrak{H}_i & I \\ * & \mathfrak{U}_i \end{bmatrix} \geqslant 0 \ (i = 1, 2, 3),$$
$$\begin{bmatrix} \mathcal{L}_j & I \\ * & T_j \end{bmatrix} \geqslant 0, \quad \begin{bmatrix} \mathcal{W}_j & I \\ * & \mathcal{Z}_j \end{bmatrix} \geqslant 0 \ (j = 1, 2),$$

where $\mathcal{M}_{22} = \text{diag}\{-\mathfrak{U}_1, -\mathfrak{U}_2, -\mathfrak{U}_3, -\mathcal{Z}_1, -\mathcal{Z}_2\}$.

Remark 3.6. If we set $\omega_1(t) = 0$ and $\omega_2(t) = 0$, the error system (2.9) becomes

$$\dot{\epsilon}(t) = A_1\epsilon_i(t) + A_2\epsilon_i(t - \tau(t)) + Bg(\epsilon_i(t)) + (1 - \varphi)G(t) + c(A \otimes D)\epsilon(t) + \bar{K}\epsilon_i(t - \rho(t)). \tag{3.21}$$

The following theorem has suitable conditions for the healthy CACS and diseased CACS in CDNs without the disturbance.

Theorem 3.7. *For given positive scalars* τ, ρ, μ_1, μ_2, υ, *any matrix* G_1, G_2, *the error system* (3.21) *is exponentially synchronized by the feedback controller* (2.7), *if there exist matrices* $P = \text{diag}\{P_1, P_2, \ldots, P_N\} > 0$, $R_1 > 0$, $R_2 > 0$, $R_3 > 0$, $R_4 > 0$, $Q_1 > 0$, $Q_2 > 0$, $Q_3 > 0$, $T_1 > 0$, $T_2 > 0$, $X = \text{diag}\{X_1, X_2, \ldots, X_N\}$, *for any matrix* Q *with appropriate dimension such that the following conditions hold:*

$$\begin{bmatrix} Q_3 & Q \\ * & Q_3 \end{bmatrix} \geqslant 0, \quad \tilde{\Pi} = \begin{bmatrix} \tilde{\Pi}_{11} & \tilde{\Pi}_{12} \\ * & \tilde{\Pi}_{22} \end{bmatrix} < 0,$$

where

$$\tilde{\Pi}_{11} = \vartheta_1 + \vartheta_2 + \vartheta_3 + \vartheta_4 + \vartheta_5 - \upsilon\Gamma_{11}^T \begin{bmatrix} \bar{G}_1 & \bar{G}_2 \\ * & I \end{bmatrix} \Gamma_{11},$$

$$\tilde{\Pi}_{12} = [\tau\tilde{\Upsilon}^T, \rho\tilde{\Upsilon}^T, \rho\tilde{\Upsilon}^T, \frac{\tau}{\sqrt{2}}\tilde{\Upsilon}^T, \frac{\rho}{\sqrt{2}}\tilde{\Upsilon}^T],$$
$$\tilde{\Pi}_{22} = \text{diag}\{-2P + Q_1, -2P + Q_2, -2P + Q_3, -2P + T_1, -2P + T_2\},$$
$$\tilde{\Upsilon} = PA_1e_1 + PA_2e_2 + PBe_{12} + Pc(A \otimes D)e_1 + Xe_4,$$

and the definitions for the additional variables match those in Theorem 3.4. In addition, the gain matrices of the necessary controllers are provided by $\bar{K} = P^{-1}X$.

Proof. According to Theorem 3.4, the proof of this theorem follows. □

4. Numerical examples

Example 4.1. Consider the isolated node (2.3) and diseased CACS in CDNs (2.2) with three nodes. The parameters of the isolated node (2.3) and diseased CACS in CDNs (2.2) are as follows:

$$A_1 = \begin{bmatrix} -0.1 & 1.5 \\ 0.55 & -0.25 \end{bmatrix}, \quad A_2 = \begin{bmatrix} -0.05 & 0.2 \\ 0.025 & -0.1 \end{bmatrix}, \quad B = \begin{bmatrix} 0 & 0 \\ 0 & -0.4 \end{bmatrix}, \quad E = \text{diag}\{1, 1, 1, 1, 1, 1\}.$$

Assuming the outer-coupling matrix to be $A = (a_{ij})_{3\times3}$ and inner-coupling matrix D to be shown as follows:

$$A = \begin{bmatrix} -2 & 1 & 1 \\ 1 & -2 & 1 \\ 1 & 1 & -2 \end{bmatrix}, \quad D = \begin{bmatrix} 1 & 0 \\ 0 & 1 \end{bmatrix}.$$

In this example, we choose G_1, G_2 as $G_1 = \begin{bmatrix} 0.05 & 0.05 \\ 0.05 & 0.05 \end{bmatrix}$, $G_2 = \begin{bmatrix} -0.05 & 0.05 \\ -0.15 & -0.25 \end{bmatrix}$. The time-varying delay is given as $\tau(t) = 0.2 + 0.05\sin(10t)$ and $\rho(t) = 0.3 + 0.05\sin(t)$. A simple computing determines $\tau = 0.25$, $\rho = 0.35$ $\mu_1 = 0.5$, $\mu_2 = 0.7$, $c = 0.5$. The linear matrix inequalities (LMIs) in Theorem 3.4 are solved in Matlab using the LMIs toolbox to get the controller matrices shown below,

$$K_1 = \begin{bmatrix} -0.6064 & 0.0471 \\ -0.1643 & -0.2683 \end{bmatrix}, \quad K_2 = \begin{bmatrix} -0.6064 & 0.0471 \\ -0.1643 & -0.2683 \end{bmatrix}, \quad K_3 = \begin{bmatrix} -0.6064 & 0.0471 \\ -0.1643 & -0.2683 \end{bmatrix}.$$

Numerical simulations are performed to demonstrate the effectiveness of the techniques presented in this part.

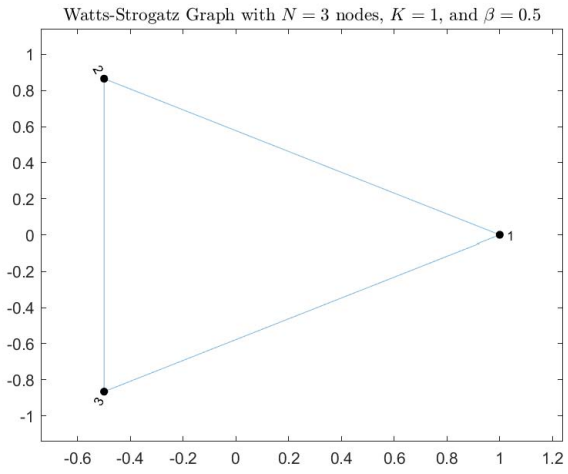

Figure 3: The coupling matrix A's topology in Example 4.1.

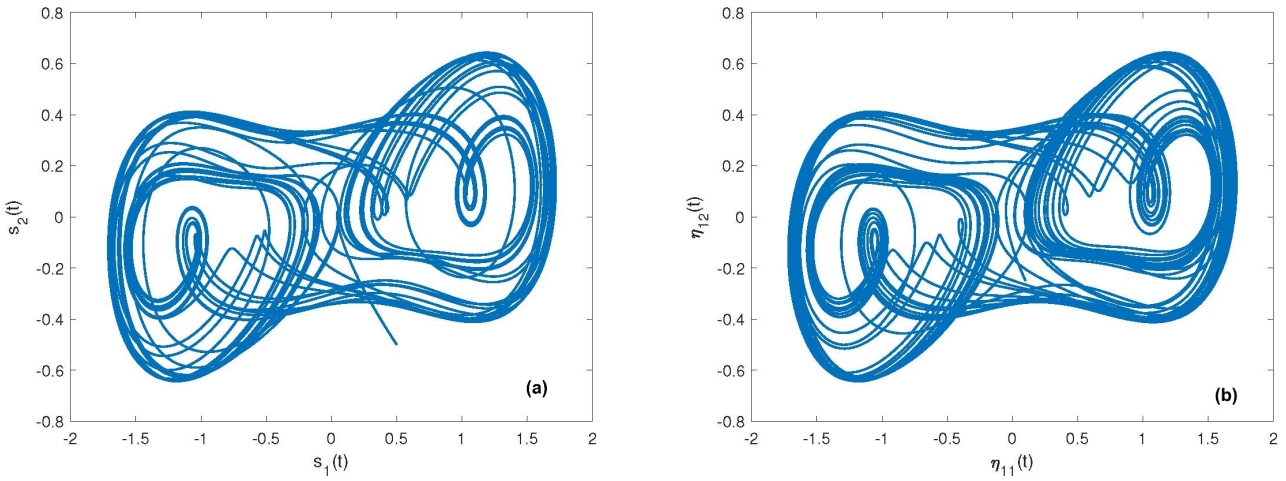

Figure 4: (a) The chaotic behavior of isolated node in Example 4.1 under $\omega_1(t) = 0$ without the control input. (b) The chaotic behavior of the diseased CACS in CDNs in Example 4.1 under $\omega_2(t) = 0$ without the control input.

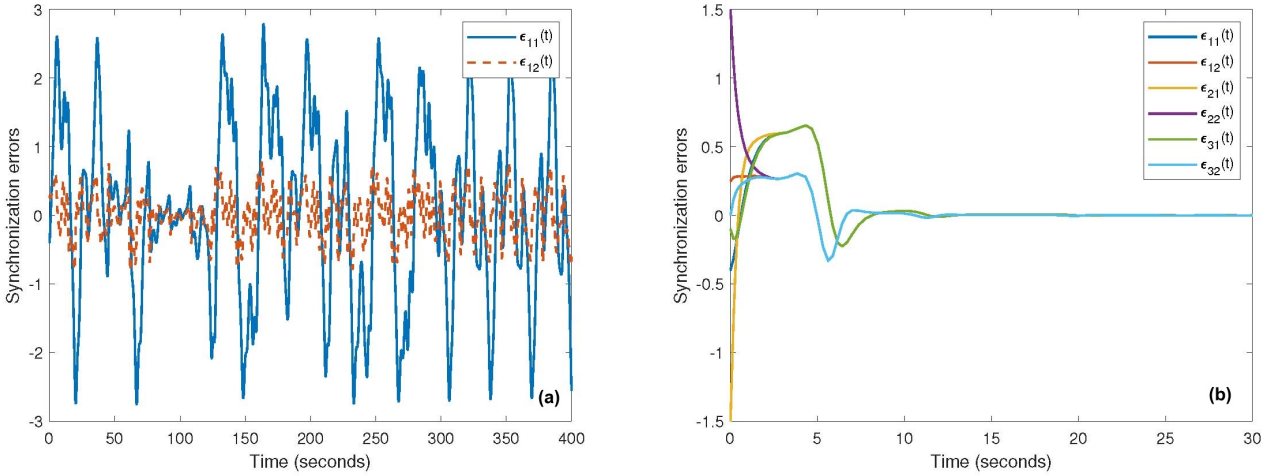

Figure 5: (a) System behavior error without control input when $\omega(t) = 0$. (b) System behavior error with control input when $\omega(t) = 0$.

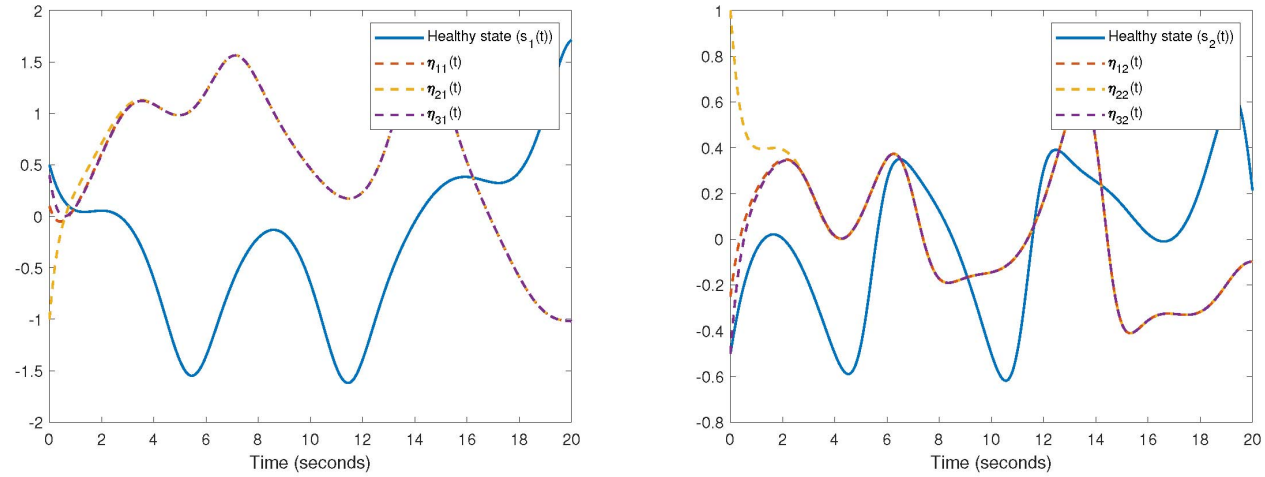

Figure 6: Response of the state for the isolate node and diseased CACS without feedback control.

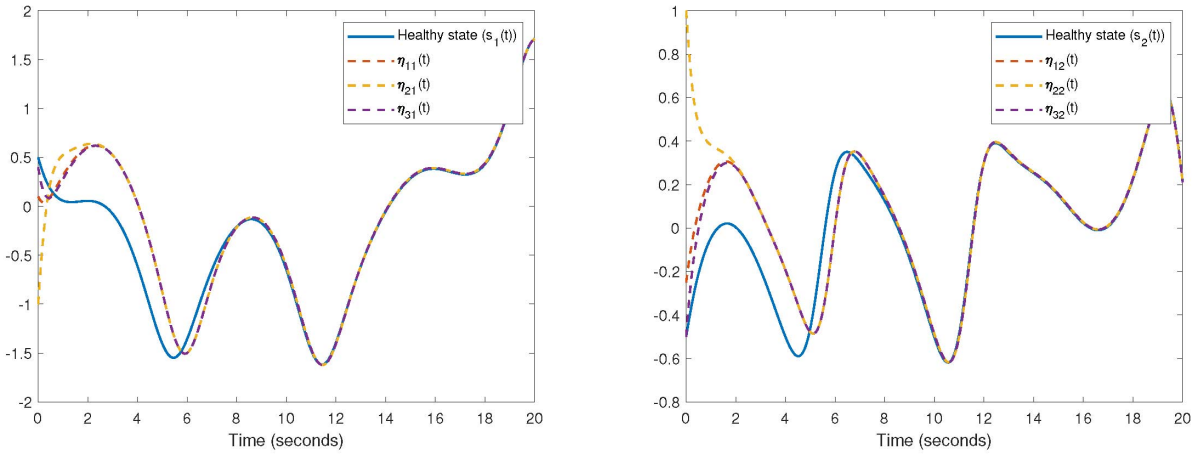

Figure 7: Response of the state for the isolate node and diseased CACS with feedback control.

Figure 3 shows the coupling matrix A's topology in Example 4.1. Figure 4 (a) shows the phase portraits of isolated node (2.3) in Example 4.1 under $\omega_1(t) = 0$ without the control input. Figure 4 (b) shows the phase portraits of the diseased CACS in CDNs (2.2) under $\omega_2(t) = 0$ without the control input. Figure 5 (a) plots the error systems between the isolated node and the diseased CACS in CDNs without the controller when $\omega(t) = 0$. Figure 5 (b) shows the error systems between the isolated node and the diseased CACS in CDNs with the control input when $\omega(t) = 0$. The patient's gender, age, and emotional state will all impact how quickly the medicine is absorbed during a natural treatment. We must support the efficacy of treatment in other situations. Figure 6 shows the error systems between the isolated node and the diseased CACS in CDNs without the feedback control. The efficacy of our strategy is seen in Figure 7. From Figure 7, it is clear that the control input can successfully synchronize the diseased system with the healthy system briefly.

Example 4.2. Consider the healthy CACS and diseased CACS in CDNs with 10 nodes and without the disturbance. The following is a presentation of the healthy CACS with state time-varying delays:

$$\dot{s}(t) = A_1 s(t) + A_2 s(t - \tau(t)) + Bf(s(t)) + G(t). \tag{4.1}$$

The diseased CACS in CDNs with the coupling for 10 nodes and input time-varying delays is shown as follows:

$$\dot{\eta}_i(t) = A_1\eta_i(t) + A_2\eta_i(t - \tau(t)) + Bf(\eta_i(t)) + G(t) + c\sum_{j=1}^{N} a_{ij}D\eta_i(t) + u_i(t - \rho(t)). \tag{4.2}$$

The following is the parameters of the healthy CACS (4.1) and diseased CACS in CDNs (4.2):

$$A_1 = \begin{bmatrix} -0.1 & 1.5 \\ 0.55 & -0.25 \end{bmatrix}, \quad A_2 = \begin{bmatrix} -0.05 & 0.2 \\ 0.025 & -0.1 \end{bmatrix}, \quad B = \begin{bmatrix} 0 & 0 \\ 0 & -0.4 \end{bmatrix}.$$

Assuming the outer-coupling matrix to be $A = (a_{ij})_{10\times 10}$ and inner-coupling matrix D are shown as follows:

$$A = \begin{bmatrix} -6 & 1 & 1 & 0 & 1 & 1 & 0 & 1 & 0 & 1 \\ 1 & -3 & 0 & 0 & 1 & 0 & 0 & 0 & 1 & 0 \\ 1 & 0 & -5 & 1 & 1 & 0 & 1 & 0 & 1 & 0 \\ 0 & 0 & 1 & -2 & 0 & 0 & 0 & 1 & 0 & 0 \\ 1 & 1 & 1 & 0 & -5 & 0 & 1 & 1 & 0 & 0 \\ 1 & 0 & 0 & 0 & 0 & -4 & 1 & 0 & 1 & 1 \\ 0 & 0 & 1 & 0 & 1 & 1 & -4 & 0 & 1 & 0 \\ 1 & 0 & 0 & 1 & 1 & 0 & 0 & -4 & 1 & 0 \\ 0 & 1 & 1 & 0 & 0 & 1 & 1 & 1 & -5 & 0 \\ 1 & 0 & 0 & 0 & 0 & 1 & 0 & 0 & 0 & -2 \end{bmatrix}, \quad D = \begin{bmatrix} 0.1 & 0 \\ 0 & 0.1 \end{bmatrix}.$$

In this example, we choose G_1, G_2 as $G_1 = \begin{bmatrix} 0.05 & 0.05 \\ 0.05 & 0.05 \end{bmatrix}$, $G_2 = \begin{bmatrix} -0.05 & 0.05 \\ -0.15 & -0.25 \end{bmatrix}$. The time-varying delay is given as $\tau(t) = 0.2 + 0.05\sin(10t)$ and $\rho(t) = 0.3 + 0.05\sin(t)$. A simple computing determines $\tau = 0.25$, $\rho = 0.35$ $\mu_1 = 0.5$, $\mu_2 = 0.7$, $c = 0.5$. The LMIs in Theorem 3.7 are solved in Matlab using the LMIs toolbox to get the controller matrices shown below,

$$K_1 = \begin{bmatrix} -0.9559 & -0.0362 \\ -0.1159 & -0.9785 \end{bmatrix}, \quad K_2 = \begin{bmatrix} -0.8211 & -0.0878 \\ 0.0907 & -1.0472 \end{bmatrix}, \quad K_3 = \begin{bmatrix} -0.9417 & -0.0408 \\ -0.0999 & -0.9957 \end{bmatrix},$$
$$K_4 = \begin{bmatrix} -0.7148 & -0.1258 \\ 0.2474 & -1.0864 \end{bmatrix}, \quad K_5 = \begin{bmatrix} -0.9416 & -0.0413 \\ -0.0968 & -0.9946 \end{bmatrix}, \quad K_6 = \begin{bmatrix} -0.9017 & -0.0609 \\ -0.0344 & -1.0192 \end{bmatrix},$$
$$K_7 = \begin{bmatrix} -0.8988 & -0.0566 \\ -0.0204 & -1.0085 \end{bmatrix}, \quad K_8 = \begin{bmatrix} -0.9072 & -0.0584 \\ -0.0515 & -1.0237 \end{bmatrix}, \quad K_9 = \begin{bmatrix} -0.9464 & -0.0394 \\ -0.1124 & -0.9982 \end{bmatrix},$$
$$K_{10} = \begin{bmatrix} -0.7137 & -0.1203 \\ 0.2535 & -1.0766 \end{bmatrix}.$$

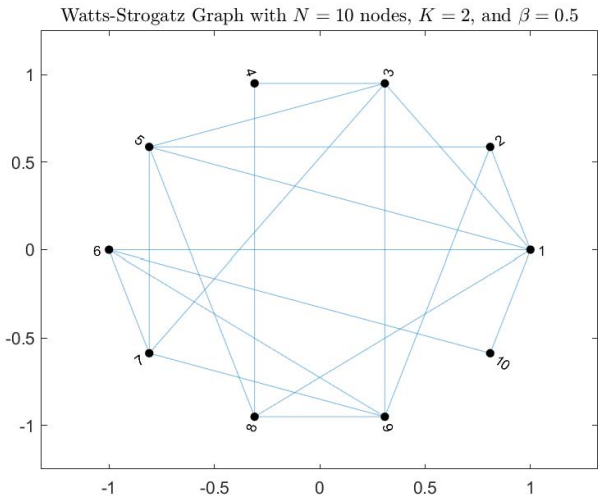

Figure 8: The coupling matrix A's topology in Example 4.2.

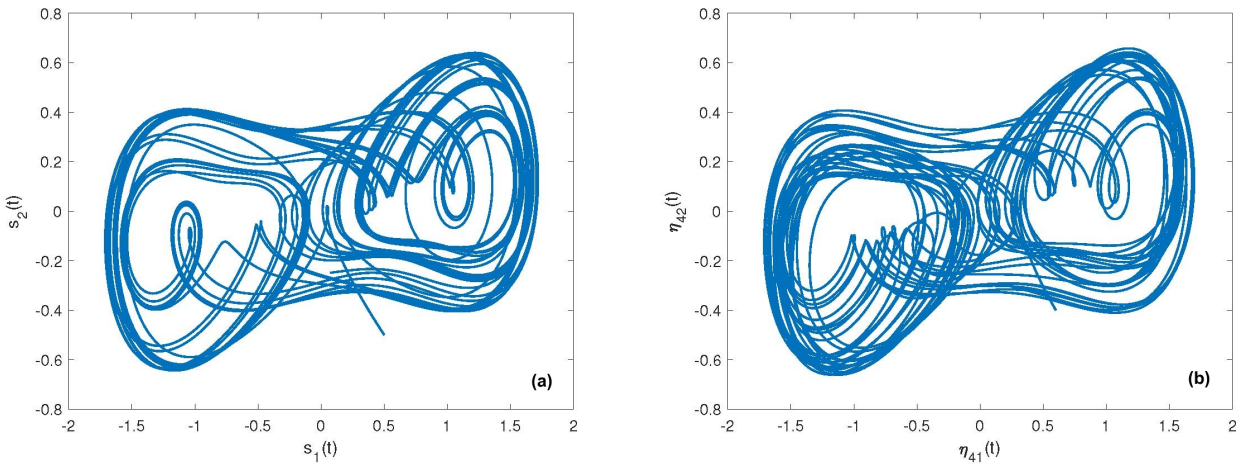

Figure 9: (a) The isolated node's chaotic behavior in Example 4.2 under $\omega_1(t) = 0$ without the control input. (b) The diseased CACS in CDNs's chaotic behavior in Example 4.2 under $\omega_2(t) = 0$ without the control input.

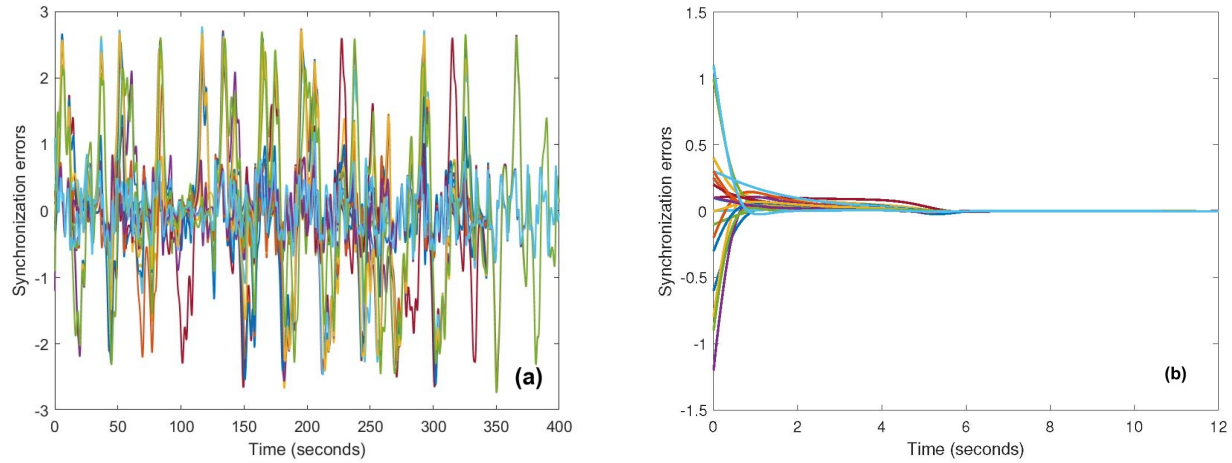

Figure 10: (a) System behavior error under $\omega(t) = 0$ without control input. (b) System behavior error under $\omega(t) = 0$ with control input.

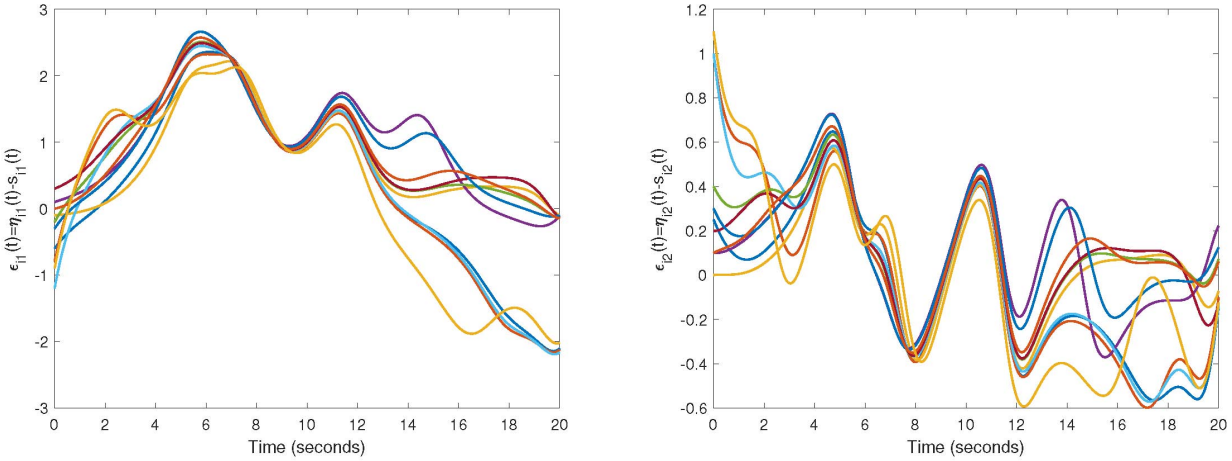

Figure 11: The synchronization errors between the states of isolate node $s(t)$ (4.1) and node $\eta_i(t)$ (4.2), $i = 1, 2, \ldots, 10$, without feedback control (2.7).

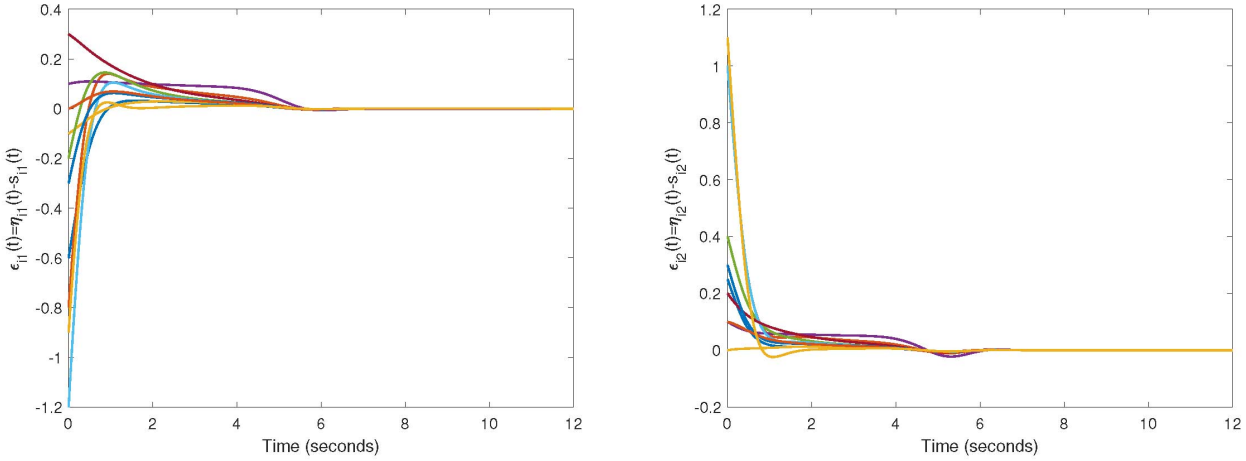

Figure 12: The synchronization errors between the states of isolate node $s(t)$ (4.1) and node $\eta_i(t)$ (4.2), $i = 1, 2, \ldots, 10$, with feedback control (2.7).

Figure 8 shows the coupling matrix A's topology in Example 4.2. Figure 9 (a) shows the phase portraits of isolated node (2.3) in Example 4.2 under $\omega_1(t) = 0$ without the control input. Figure 9 (b) shows the phase portraits of the diseased CACS in CDNs (4.2) under $\omega_2(t) = 0$ without the controller input. The error systems between the isolated node and the diseased CACS in CDNs without the controller input are depicted in Figure 10 (a). Figure 10 (b) illustrates the error systems between the diseased CACS in CDNs and the isolated node. Figure 11 plots the synchronization errors between the states of isolate node $s(t)$ (4.1) and node $\eta_i(t)$ (4.2), $i = 1, 2, \ldots, 10$, without feedback control (2.7). The synchronization errors between the states of isolate node $s(t)$ (4.1) and node $\eta_i(t)$ (4.2), $i = 1, 2, \ldots, 10$, with feedback control (2.7) are shown in Figure 12.

Remark 4.3. We have a positive coupling strength constant c and an inner coupling matrix D, an advantage of these numerical simulations. Additionally, we continue to research CACS in CDNs with input and state time-varying delays. Therefore, these simulations cannot use the stability conditions established in [13, 18, 22, 35, 41].

5. Conclusions

The problem of exponential synchronization of the CACS in CDNs with state and input time-varying delays is being investigated for the first time. Notably, the dependable controller was built to inhibit irregular heart rhythms, essential for providing the heart with nutrition and oxygen throughout the day. This contrasts with unpredictability, such as drug use, emotional instability, etc. The improved double/triple integral inequalities and stability criterion conditions were in the form of LMIs due to the construction of a new LKF and the application of Jensen inequality and Wirtinger-based integral inequality, which was enough to guarantee that the diseased system coordinates with the health system for a brief period of time. The numerical simulations demonstrated that our synchronization technique successfully synchronizes the spasm coronary system with the healthy circulatory system under input delay and perturbation. In future work, the findings and techniques presented in this study are anticipated to be extended and adapted to a wide range of real-world systems and practical applications, for example, adaptive control [7, 11, 18, 27], H_∞ control [6, 21–23, 39], mixed passive and H_∞ performance index [13], fuzzy control [32], observer-based control [41], and state-feedback control [35].

Use of AI tools declaration

The authors declare they have not used Artificial Intelligence (AI) tools in the creation of this article.

Acknowledgments

This work was supported by Rajamangala University of Technology Isan under the Science Research and Innovation Fund. Agreement No. FF68/NKR/035.

References

[1] M. S. Ali, J. Yogambigai, *Synchronization of complex dynamical networks with hybrid coupling delays on time scales by handling multitude Kronecker product terms*, Appl. Math. Comput., **291** (2016), 244–258. 1

[2] P. Anbalagan, Z. Feng, T. Huang, Y. Cui, *Mean-square synchronization of additive time-varying delayed Markovian jumping neural networks under multiple stochastic sampling*, IEEE Trans. Neural Netw. Learn., **36** (2025), 11928–11942. 1

[3] P. Anbalagan, J. H. Jeong, Y. H. Joo, *Secure reachable set synthesis and reliable event-driven mechanism for T–S fuzzy semi-Markovian networked control systems against deception attacks*, IEEE Trans. Fuzzy Syst., **32** (2024), 3928–3942. 1

[4] T. Botmart, N. Yotha, P. Niamsup, W. Weera, *Hybrid adaptive pinning control for function projective synchronization of delayed neural networks with mixed uncertain couplings*, Complexity, **2017** (2017), 18 pages. 1

[5] X. Cai, S. Zhong, J. Wang, K. Shi, *Robust H_∞ control for uncertain delayed T-S fuzzy systems with stochastic packet dropouts*, Appl. Math. Comput., **385** (2020), 21 pages. 1

[6] C. Chantawat, T. Botmart, *Finite-time H_∞ synchronization control for coronary artery chaos system with input and state time-varying delays*, PLoS ONE, **17** (2022), 1–21. 1, 2.4, 5

[7] B. Du, Q. Xu, J. Zhang, Y. Tang, L. Wang, R. Yuan, Y. Yuan, J. An, *Periodic intermittent adaptive control with saturation for pinning quasi-consensus of heterogeneous multi-agent systems with external disturbances*, Entropy, **25** (2023), 20 pages. 1, 5

[8] L. Faybusovich, T. Mouktonglang, *Multi-target linear-quadratic control problem and second-order cone programming*, Syst. Control Lett., **52** (2004), 17–23. 1

[9] L. Faybusovich, T. Mouktonglang, T. Tsuchiya, *Implementation of infinite-dimensional interior-point method for solving multi-criteria linear-quadratic control problem*, Optim. Methods Softw., **21** (2006), 315–341. 1

[10] K. Gu, J. Chen, V. L. Kharitonov, *Stability of time-delay systems*, Birkhäuser Boston, Boston, (2003). 1

[11] J. Guo, Z. Zhao, J. Zhang, G. Ding, *Adaptive observation control for synchronization of coronary artery time-delay systems*, Mod. Phys. Lett. B, **33** (2019), 21 pages. 1, 5

[12] Q.-L. Han, *Absolute stability of time-delay systems with sector-bounded nonlinearity*, Automatica J. IFAC, **41** (2005), 2171–2176. 1

[13] S. Harshavarthini, R. Sakthivel, F. Kong, *Finite-time synchronization of chaotic coronary artery system with input time-varying delay*, Chaos Solitons Fractals, **134** (2020), 8 pages. 1, 2.2, 3.2, 4.3, 5

[14] A. Hongsri, T. Botmart, W. Weera, *Improved on extended dissipative analysis for sampled-data synchronization of complex dynamical networks with coupling delays*, IEEE Access, **10** (2022), 108625–108640. 1

[15] A. Hongsri, T. Botmart, W. Weera, P. Junsawang, *New delay-dependent synchronization criteria of complex dynamical networks with time-varying coupling delay based on sampled-data control via new integral inequality*, IEEE Access, **9** (2021), 64958–64971. 1, 2.3, 2.5

[16] D. H. Ji, J. H. Park, W. J. Yoo, S. C. Won, S. M. Lee, *Synchronization criterion for Lur'e type complex dynamical networks with time-varying delay*, Phys. Lett. A, **374** (2010), 1218–1227. 1

[17] X. Jiang, Q.-L. Han, *New stability criteria for linear systems with interval time-varying delay*, Automatica J. IFAC, **44** (2008), 2680–2685. 1

[18] W. Li, *Tracking control of chaotic coronary artery system*, Int. J. Syst. Sci., **43** (2012), 21–30. 1, 2.2, 4.3, 5

[19] C. Li, G. Chen, *Synchronization in general complex dynamical networks with coupling delays*, Phys. A., **343** (2004), 263–278. 1

[20] X.-F. Li, Y.-D. Chu, A. Y. T. Leung, H. Zhang, *Synchronization of uncertain chaotic systems via complete-adaptive-impulsive controls*, Chaos Solitons Fractals, **100** (2017), 24–30. 1

[21] B. Li, Z. Zhao, R. Wang, G. Ding, *Synchronization control design based on Wirtinger inequality for uncertain coronary artery time-delay system with input saturation*, IEEE Access, **7** (2009), 76611–76619. 1, 3.2, 5

[22] X.-M. Li, Z.-S. Zhao, J. Zhang, L.-K. Sun, *H_∞ synchronization of the coronary artery system with input time-varying delay*, Chinese Phys. B, **25** (2016). 1, 2.2, 4.3

[23] S. S. Li, Z. S. Zhao, J. Zhang, J. Sun, L. K. Sun, *H_∞ control of coronary artery input time-delay system via the free-matrix-based integral inequality*, Math. Probl. Eng., **2018** (2018), 12 pages. 1, 5

[24] P. Niamsup, T. Botmart, W. Weera, *Modified function projective synchronization of complex dynamical networks with mixed time-varying and asymmetric coupling delays via new hybrid pinning adaptive control*, Adv. Difference Equ., **2017** (2017), 31 pages. 1

[25] F. Nian, X. Wang, *Chaotic synchronization of hybrid state on complex networks*, Int. J. Mod. Phys. C, **21** (2010), 457–469. 1

[26] P. Park, J. W. Ko, C. Jeong, *Reciprocally convex approach to stability of systems with time-varying delays*, Automatica J. IFAC, **47** (2011), 235–238. 1

[27] X. Quan, X. Xu, S. Zhuang, J. Xiao, C. Song, C. Che, *New complex projective synchronization strategies for drive-response networks with fractional complex-variable dynamics*, Appl. Math. Comput., **338** (2018), 552–566. 1, 5

[28] S. A. Samy, J. H. Jeong, Y. H. Joo, *Reachable set performance and quantized sampled-data synchronization analysis of neural networks under random packet dropouts via enhanced looped functional*, Expert Syst. Appl., **252** (2024). 1

[29] A. Stephen, K. Rajakopal, R. Raja, A. Srinidhi, K. Thamilmaran, R. P. Agarwal, *Non-fragile reliable control for multi-agent systems with actuator faults using an improved L-K functional*, Nonlinear Dyn., **113** (2025), 6645–6669. 1

[30] J. Sun, G. P. Liu, J. Chen, D. Rees, *Improved delay-range-dependent stability criteria for linear systems with time-varying delays*, Automatica J. IFAC, **46** (2010), 466–470. 1

[31] Y. Tang, H. Gao, W. Zou, J. Kurths, *Distributed synchronization in networks of agent systems with nonlinearities and random switchings*, IEEE Trans. Cybern., **43** (2013), 358–370. 1

[32] R. Wang, B. Li, Z. S. Zhao, J. Guo, Z. Zhu, *Synchronization of fuzzy control design based on Bessel-Legendre inequality for coronary artery state time-delay system*, IEEE Access, **7** (2019), 181933–181941. 1, 3.2, 5

[33] W. Wang, H.-B. Zeng, *A Looped Functional Method to Design State Feedback Controllers for Lurie Networked Control Systems*, IEEE CAA J. Autom. Sinica, **10** (2023), 1093–1095. 3.5

[34] Z.-G. Wu, J. H. Park, H. Su, B. Song, J. Chu, *Exponential synchronization for complex dynamical networks with sampled-data*, J. Franklin Inst., **349** (2012), 2735–2749. 1, 2.6

[35] W. S. Wu, Z. S. Zhao, J. Zhang, L. K. Sun, *State feedback synchronization control of coronary artery chaos system with interval time-varying delay*, Nonlinear Dyn., **87** (2017), 1773–1783. 1, 2.2, 4.3, 5

[36] Z. Xu, X. Li, P. Duan, *Synchronization of complex networks with time-varying delay of unknown bound via delayed*

impulsive control, Neural Netw., **125** (2020), 224–232. 1

[37] Z. Xu, D. Peng, X. Li, *Synchronization of chaotic neural networks with time delay via distributed delayed impulsive control*, Neural Netw., **118** (2019), 332–337. 1

[38] M. Xu, J.-L. Wang, Y.-L. Huang, P.-C. Wei, S.-X. Wang, *Pinning synchronization of complex dynamical networks with and without timevarying delay*, Neurocomputing, **266** (2017), 263–273. 1

[39] J. Zhang, S. S. Li, Z. Zhao, J. Sun, *Improved synchronization criteria for coronary artery input time-delay system*, IEEE Access, **6** (2018), 68221–68232. 1, 3.2, 5

[40] G. Zhang, Z. Liu, Z. Ma, *Synchronization of complex dynamical networks via impulsive control*, Chaos, **17** (2007), 9 pages. 1

[41] Z. Zhao, Y. Du, J. Zhang, L. Sun, *Observer-based H_∞ synchronization control for input and output time-delays coronary artery system*, Asian J. Control, **21** (2019), 1142–1152. 1, 2.2, 3.2, 4.3, 5

[42] N. Zhao, C. Lin, B. Chen, Q.-G. Wang, *A new double integral inequality and application to stability test for time-delay systems*, Appl. Math. Lett., **65** (2017), 26–31. 2.7

[43] C. Zhao, S. Zhong, Q. Zhong, K. Shi, *Synchronization of Markovian complex networks with input mode delay and Markovian directed communication via distributed dynamic event-triggered control*, Nonlinear Anal. Hybrid Syst., **36** (2020), 14 pages. 1

[44] J. Zhou, Q. Wu, L. Xiang, *Impulsive pinning complex dynamical networks and applications to firing neuronal synchronization*, Nonlinear Dyn., **69** (2012), 1393–1403. 1